Choriocapillaris Flow Deficits and Treatment-Naïve Macular Neovascularization Secondary to Age-Related Macular Degeneration

Jackson M. Scharf,[1,2] Giulia Corradetti,[1,3] Ahmed Roshdy Alagorie,[3,4] Christelle Grondin,[1] Assaf Hilely,[1,5] Derrick Wang,[1] SriniVas Sadda,[3,6] and David Sarraf[1,6,7]

[1]Retina Disorders and Ophthalmic Genetics, Stein Eye Institute, University of California-Los Angeles, Los Angeles, California, United States
[2]Vagelos College of Physicians and Surgeons, Columbia University, New York, New York, United States
[3]Doheny Image Reading Center, Doheny Eye Institute, University of California Los Angeles (UCLA) Affiliated, Los Angeles, California, United States
[4]Department of Ophthalmology, Faculty of Medicine, Tanta University, Tanta, Egypt
[5]Division of Ophthalmology, Tel Aviv Medical Center, Sackler Faculty of Medicine, Tel Aviv University, Tel Aviv, Israel
[6]Department of Ophthalmology, David Geffen School of Medicine at UCLA, Los Angeles, California, United States
[7]Greater Los Angeles VA Healthcare Center, Los Angeles, California, United States

Correspondence: David Sarraf, Stein Eye Institute, University of California Los Angeles, 100 Stein Plaza, Los Angeles, CA 90095, USA; dsarraf@jsei.ucla.edu.

JMS and GC contributed equally to this work.

Received: April 1, 2020
Accepted: August 5, 2020
Published: September 9, 2020

Citation: Scharf JM, Corradetti G, Alagorie AR, et al. Choriocapillaris flow deficits and treatment-naïve macular neovascularization secondary to age-related macular degeneration. *Invest Ophthalmol Vis Sci.* 2020;61(11):11. https://doi.org/10.1167/iovs.61.11.11

Purpose. To evaluate choriocapillaris (CC) flow deficits (FD) in eyes with treatment-naïve macular neovascularization (MNV) and to compare CC FD around exudative versus nonexudative MNV.

Methods. Treatment-naïve eyes with a diagnosis of either exudative or nonexudative AMD and type 1 MNV were included. Normal control eyes were age-matched to each AMD eye one to one. En face optical coherence tomography angiograms were analyzed for percentage of CC FD (FD%) in two concentric 500 µm rings, ring 1 and ring 2, surrounding the dark halo around MNV. The mean CC FD% in ring 1 and ring 2 was evaluated for each eye. A secondary analysis was similarly carried out to investigate the differences in CC FD% in exudative versus nonexudative treatment-naïve MNV.

Results. Twenty-three eyes with treatment-naïve MNV were age matched with 23 normal controls. The mean CC FD% was significantly greater in both rings in the MNV versus the normal control group ($P < 0.05$) and was significantly greater in the inner ring, closer to the lesion, than the outer ring. The mean FD% was also greater in both rings in the exudative versus the nonexudative MNV group, but this difference did not reach statistical significance.

Conclusions. The CC FD% was greater in the area surrounding MNV versus age-matched normal controls and in the ring closer to the MNV lesion. Further, CC FD was greater in eyes with exudative versus nonexudative MNV in both rings surrounding the associated dark halo, although this difference was not statistically significant.

Keywords: macular neovascularization, choriocapillaris, flow deficits, optical coherence tomography angiography, age-related macular degeneration

The process of macular neovascularization (MNV) secondary to AMD can be associated with significant disruption of the choriocapillaris (CC) in the area surrounding the MNV[1,2] and CC impairment may be the initial insult that drives MNV formation, suggesting that neovascular AMD may be a vascular disease with secondary RPE and photoreceptor degeneration owing to CC damage.[1,3,4] Recent optical coherence tomography angiography (OCTA) studies have shown that eyes with geographic atrophy exhibit greater CC flow deficits (FD) versus normal eyes and versus eyes with neovascular AMD and that CC impairment may predict the progression of geographic atrophy (GA).[5–7]

MNV secondary to AMD is usually complicated by sub-RPE, subretinal or intraretinal exudation that must be treated with anti-VEGF injection.[8] Green et al[9] and Sarks[10] were the first to describe choroidal neovascularization in post mortem eyes in the absence of associated exudation. This condition has been clinically referred to as quiescent or nonexudative MNV and was originally described with the aid of indocyanine green angiography and more recently with OCTA.[11–13] The pathophysiologic mechanisms differentiating exudative versus non exudative MNV are unclear, but identification of these factors may provide guidance with management.

The advent of OCTA has provided the capability to more accurately study the CC and MNV in vivo at a high resolution without the need for dye injection, by performing CC FD analysis.[14,15] Several studies have investigated FD of the

CC in the perilesional low-flow dark halo (DH) surrounding MNV using en face OCTA analysis.[1,16–19]

The primary aim of this study was to perform a CC FD analysis surrounding and not including the DH in eyes with both exudative and nonexudative treatment-naïve MNV due to AMD versus age-matched normal controls. A secondary analysis was to assess the differences in the CC FD percentage (FD%) in eyes with exudative versus nonexudative treatment-naïve MNV.

Methods

This study adhered to the tenets of the Declaration of Helsinki and was conducted in accordance with the regulations of the Health Insurance Portability and Accountability Act. Institutional Review Board approval was obtained from the University of California – Los Angeles (UCLA) Geffen School of Medicine.

This retrospective, cross-sectional study used the RTvue-XR Avanti spectral domain-OCTA (Optovue, Inc, Fremont, CA) system. All patients included in this study were evaluated by a single retinal specialist (DS) at the Stein Eye Institute UCLA between January 2017 and September 2019. Eligible subjects were diagnosed with AMD and treatment naïve MNV and underwent testing with 6 × 6 mm en face OCTA analysis. Normal controls were matched for age and scan quality index.

Inclusion criteria for the study included treatment-naïve eyes with a diagnosis of either exudative or nonexudative AMD and type 1 MNV imaged with en face 6 × 6 mm spectral domain OCTA. To be included in the study, all borders of the MNV were required to be localized at least 2 mm from the edge of the scan. Exclusion criteria included poor quality OCTA scans (quality index of <7 or signal strength index of <65 or significant motion artifacts, and presence of significant motion or checkerboard artifact) and/or any history of anti-VEGF injection or retinal laser therapy in the study eye. Eyes with type 2 and type 3 MNV, perifoveal exudative vascular anomalous complex, multifocal MNV, geographic atrophy and any evidence of other comorbid retinal and/or macular diseases (e.g., diabetic retinopathy, retinal venous occlusion) were also excluded. Eyes with significant media opacity, including cataract, impairing the quality of the images, and high myopic eyes with a refractive error of greater than 6 diopters were also excluded.

The RTvue-XR Avanti Optovue database at the Stein Eye Institute UCLA was searched for treatment-naïve type 1 MNV secondary to AMD and measuring 1 disc diameter or less in size. A chart review of each patient was then performed to determine if patients were treatment naïve at the time of the OCTA scan and to exclude any patients who had been treated with anti-VEGF injection(s) in the study eye. Relevant clinical history was also recorded. For each case of treatment-naïve MNV, spectral domain optical coherence tomography (OCT) volume scans were analyzed for presence of exudative features at baseline and at every subsequent visit. MNV criteria for inclusion were assessed by a first grader (JS) and confirmed by a second grader (GC).

After identification of AMD eyes with MNV that fulfilled criteria, spectral domain OCTA volume scans of normal control eyes were obtained which were age-matched to each AMD eye, in a one to one comparison, to exclude aging as a factor associated with CC FD and to ensure comparable localization of the CC FD analysis in the affected and in the age-matched control eye.[20,21] For each subject, only one eye was included in the analysis: the eye with evidence of treatment-naïve MNV in the AMD cohort and a corresponding eye for the age-matched normal control group. In addition to comparing the CC FD in MNV eyes versus age-matched controls, eyes with exudative versus nonexudative treatment naïve MNV were also compared.

Exudative MNV was defined according to the presence of subretinal or intraretinal fluid on OCT at baseline presentation. Eyes with nonexudative MNV by contrast never exhibited subretinal or intraretinal fluid at baseline or at any of the follow-up evaluations.

Image Acquisition

En face OCTA high-definition 6 × 6 mm volume scans (400 pixels × 400 pixels resolution) were acquired using the RTvue-XR Avanti (Optovue), a spectral domain OCTA (spectral domain OCTA) device that uses an A-scan rate of 70,000 scans per second, a light source centered at 840 nm and a full-width at half maximum bandwidth of 45 nm. At each location of the retina, the RTVue-XR Avanti system captures two consecutive OCTA volume scans with orthogonal fast-scan directions (horizontal and vertical), each containing 400 A-scans (at 400 B-scan locations), separated by 15 µm and then merged to minimize motion artifacts.[22,23]

Projection artifacts were partially removed using the default RTvue-XR Avanti Software in the Optovue device.[24]

Image Processing

The CC FD analysis was calculated in the different groups by analyzing en face OCTA images using Bruch's membrane as the segmentation reference. A combined approach to obtain the most optimal CC segmentation was performed that included the manufacturer's automated segmentation and manual segmentation. The automated CC slab was defined as a 10-µm-thick slab with an inner and outer boundary located 21 µm and 31 µm below the anatomic location of Bruch's membrane, respectively (Fig. 1).[25] The automatic segmentation was evaluated in every case to ensure accurate referencing of Bruch's membrane and any segmentation errors were manually corrected. Manual segmentation was facilitated by the manufacturer propagation plugin which can repeat the manually corrected segmentation for several B-scans. All en face OCTA images of the CC with corrected segmentation were exported and analyzed on ImageJ Software, using the Fiji application version 2.0.0-rc-69/1.52p (http://rsb.info.nih.gov/ij/index.html) and provided in the public domain by National Institutes of Health (Bethesda, MD).[26] All images were compensated for signal loss and shadowing effects.[27] An inverse transformation was first applied on the en face CC structural OCT image to improve the attenuated signal under drusen and improve the speckle noise of the image. Then, a multiplication between the en face CC angiograms with the corresponding inverted en face CC structural OCT slab was performed, using the algorithm proposed by Zhang et al.[28] to compensate for the shadowing effects of drusen (Fig. 2).

Two independent, masked graders (JS, GC) manually outlined the area of MNV and the associated DH in each en face CC OCTA scan for each subject included in the AMD group and the mean of measurements was considered in the analysis. The MNV was defined as the area occupied by high-flow, abnormal new vessels on the en face CC OCTA corresponding with an enhanced signal of blood flow in the

Investigative Ophthalmology & Visual Science

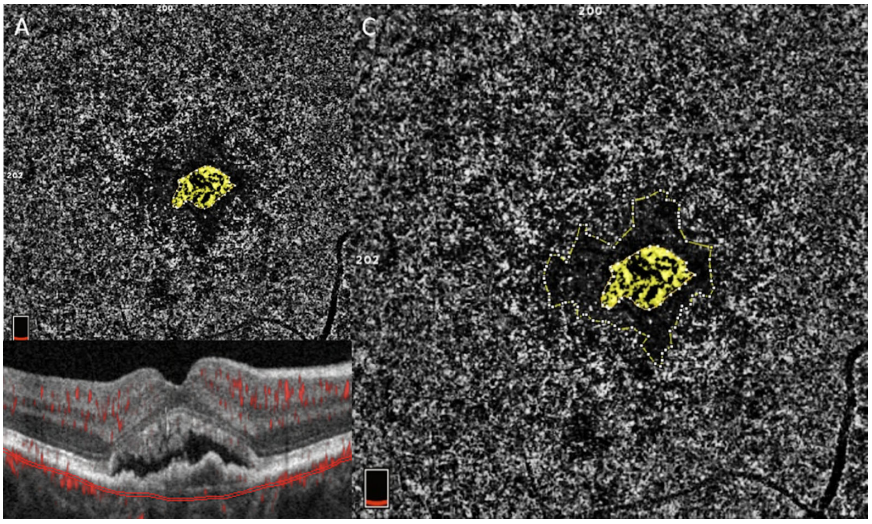

Figure 1. (**A**) The 6 × 6 mm en face CC angiogram illustrates subfoveal treatment-naïve MNV (highlighted in *yellow*). (**B**) OCT B-scan shows the corresponding CC segmentation. The Bruch's membrane offset was used to segment the CC slab, defined as a 10-µm thick slab with an inner and an outer boundary located, 21 µm and 31 µm, respectively, below the anatomic location of the Bruch's membrane. (**C**) The perilesional DH is encircled in *yellow* and is represented by a low-flow area surrounding the MNV.

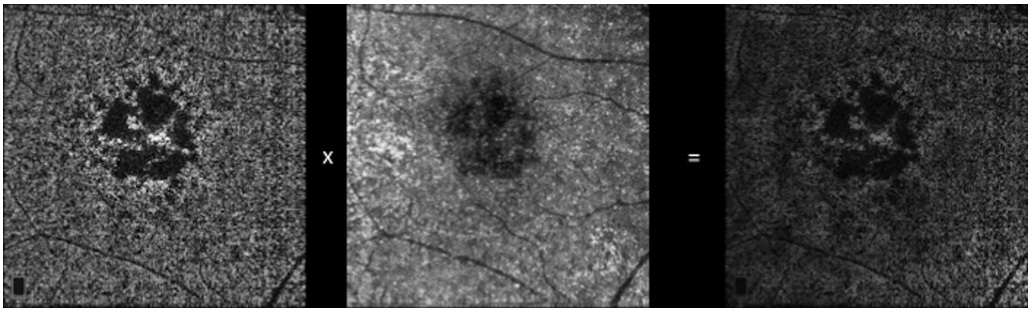

Figure 2. Compensated methodology for signal loss and shadowing effects.[31] An inverse transformation is first applied to the en face CC structural OCT image to improve the attenuated signal under drusen and improve the speckle noise of the image. Then, a multiplication between the en face CC angiogram with the corresponding inverted en face CC structural OCT slab is performed.

registered B-scan overlay, whereas the DH was defined as the low-flow area with decorrelation less than or equal to that of the foveal avascular zone immediately surrounding the MNV on the en face CC OCTA. Areas of MNV and DH were expressed in square millimeters.

The CC FD% was quantified in a 6 × 6 mm binarized image and specifically, en face CC angiograms were analyzed for percentage of FD in two concentric rings: ring 1 and ring 2 as shown in Figure 3.[15,29]

These rings spanned a 1000-µm-wide region surrounding the DH around the MNV. The CC FD% was defined as the ratio of the FD area in the region of ring 1 or ring 2 over the total scanned area in ring 1 or ring 2. To detect and isolate the areas of FD within the CC, two binarization thresholding methodologies were used: the Phansalkar local thresholding method[20,30] and the standard deviation global thresholding method.[27,28,31] Using two methodologies served to increase the generalizability of the results. With regard to the Phansalkar method, as a larger Kernel (i.e., circle) radius produces better repeatability in quantifying the CC FDs, a 43.5 µm (approximately 7.3 pixels in a 400 × 400 pixels image) Kernel radius was used to determine the local reflectivity threshold for detection of FD in this study.[27]

Regarding the standard deviation global thresholding algorithm, the threshold for FD was determined by one standard deviation from a normal database (20 subjects, 20–39 years old) as described in the previous literature.[28,31] Superficial and large retinal vessels were excluded from the CC FD% analysis using the Max Entropy plugin, the methodology for which has been detailed in previous reports.[29,32]

The CC FD% within four 1-mm^2 squares placed on the four corners of each image was computed in both the MNV and the normal control groups using the Phansalkar method to assess differences in the CC FD between MNV and normal eyes outside of ring 2. The methodology used was the same as was previously described by Alagorie et al.[33] The CC FD% measured within these peripheral regions was then compared with the CC FD% measured within ring 1 and ring 2 in MNV eyes.

Each treatment-naïve MNV eye was age matched, one to one, with a normal control eye and of note the CC extracted from the control eye was matched according to location and size of the concentric 500 µm rings in the MNV eye (Fig. 3). A primary analysis was carried out to investigate the mean CC FD% in ring 1 and ring 2 and the mean difference between ring 1 and ring 2 was evaluated for each

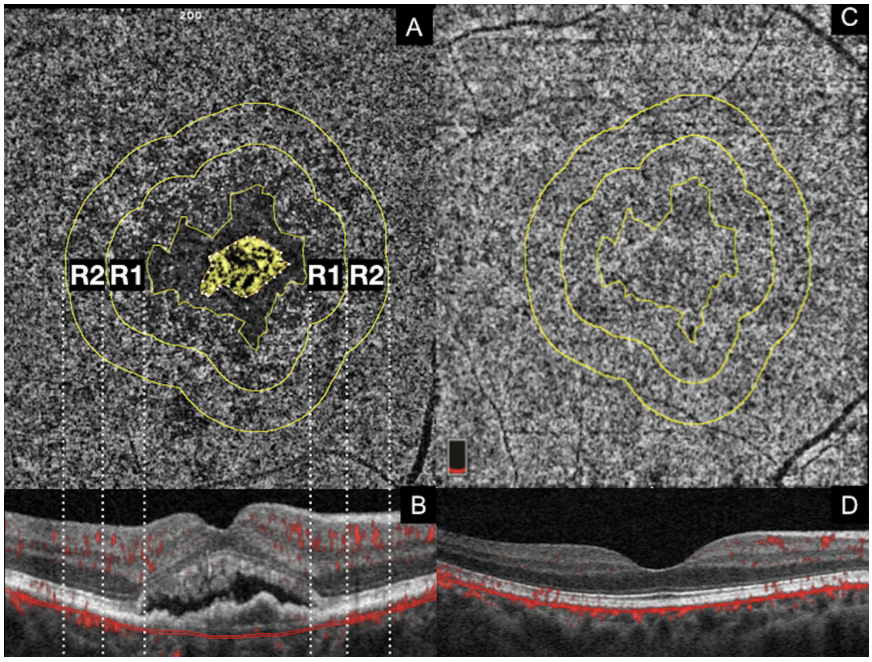

Figure 3. En face CC OCTA images are used to manually delineate MNV and the associated perilesional halo, while the rings surrounding the DH are automatically generated using the "Enlarge" plugin on ImageJ Software. (**A**) MNV is highlighted in *yellow* and the DH is represented by the low-flow area defined by an inner boundary (outer margin of the MNV) and outer boundary (inner margin of ring 1 [R1]). *Vertical dashed lines* display colocalization of the en face OCTA rings with the corresponding positions on the OCT B-scan. En face CC angiograms are analyzed for FD% in two concentric 500 µm rings, ring 1 and ring 2 [R2], spanning a 1000-µm-wide region surrounding the DH around the MNV. Each treatment-naïve MNV eye is age-matched with a normal control (**C**) and the CC is extracted from the same (location and size) concentric 500 µm rings used for the corresponding treatment-naïve MNV eye.

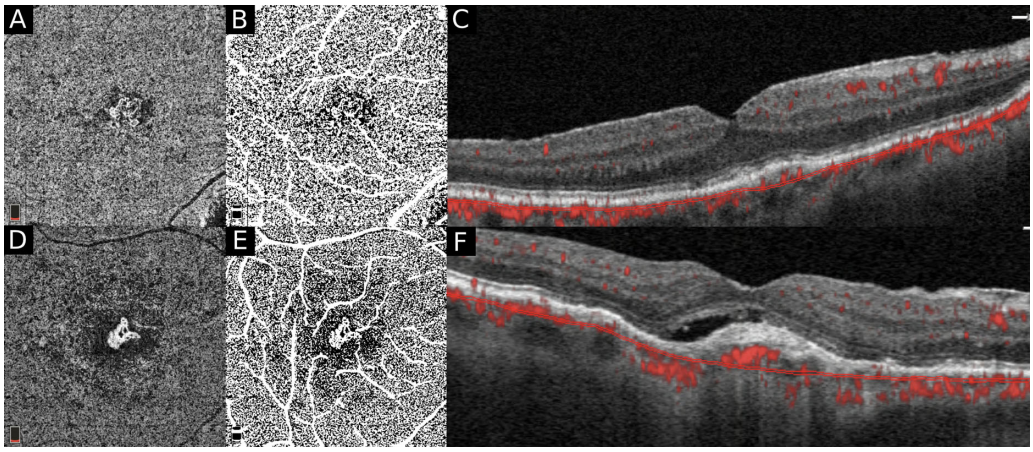

Figure 4. A subanalysis was carried out to assess the differences in the percentage (%) of CC FD in exudative versus nonexudative treatment-naïve MNV. Compensated en face CC OCTA slabs (**A**, **D**) are binarized using the Phansalkar local thresholding method (shown here) on Image J. (The standard deviation global thresholding method was also performed in this analysis to validate the Phansalkar method.) The CC FD is quantified after masking the superficial and large vessels (**D**, **E**). The B-scans (**C**, **F**) are used to determine the nature of the MNV, nonexudative (**C**) versus exudative (**F**).

eye in the AMD cohort versus the normal cohort. An additional analysis was carried out to assess the differences in the average of the CC FD% in ring 1 and ring 2 in exudative versus nonexudative treatment-naïve MNV. Each of these subgroups was also compared with the normal controls, and a mean difference between ring 1 and ring 2 was calculated (Fig. 4).

Statistical Analysis

Statistical analyses were performed using SPSS Statistics version 26 (IBM, Armonk, NY). The agreement between graders with regard to measurements of MNV and DH areas and CC FD was calculated using the two-way mixed effects intraclass correlation coefficient with a 95% confidence interval (CI) for average measurements. Descriptive

Investigative Ophthalmology & Visual Science

Table 1. OCT Angiography FD Data and Comparisons for MNV versus Age-Matched Normal Control Groups

	CC FD% R1	CC FD% R2	Δ (R1 – R2)	*P* Value
MNV cases	54.93 ± 5.70*	50.18 ± 5.70*	4.75 ± 4.58	<0.0005*
Normal Controls	42.07 ± 4.60**	40.49 ± 4.96**	1.34 ± 1.19	<0.0005**
P value (*t*-test)	<0.0005	<0.0005	<0.001	–

In ring 1, the mean CC FD% measured 54.93 ± 5.70 and 42.07 ± 4.60 in the MNV and normal control group, respectively ($P < 0.0005$). In ring 2, mean CC FD% measured 50.18 ± 5.70 and 40.49 ± 4.96 in the MNV and normal control group, respectively ($P < 0.0005$). The mean difference of CC FD% between the two rings was statistically significantly greater in the MNV eyes compared with the controls: 4.75 ± 4.58 and 1.34 ± 1.19, respectively. R1 = ring 1, R2 = ring 2.

statistics for subanalysis is reported in Table 2. Statistically significant difference was calculated between the following paired groups: treatment-naïve MNV eyes versus normal eyes, treatment-naïve exudative MNV eyes versus treatment-naïve non exudative MNV eyes, treatment-naïve exudative MNV eyes versus normal control eyes, and treatment-naïve non exudative MNV eyes versus normal controls. Statistical significant differences for age, visual acuity (VA), DH and MNV areas were also calculated in these paired-groups. The statistical significance was assessed using a *t*-test and a *P* value of less than 0.05. Data were presented as mean and standard deviation. For all eyes, VA measured using Snellen's chart was collected and was converted into a logMAR scale for statistical analysis.

Results

Of the 35 eligible eyes, 12 were excluded because of poor scan quality. Twenty-three eyes with treatment-naïve MNV (19 males, 4 females) were therefore enrolled and age matched with twenty-three normal controls (12 males, 11 females). The mean age was 79.47 ± 7.30 and 78.04 ± 5.90 ($P = 0.09$) in the treatment-naïve MNV and normal control groups, respectively. A total of 12 subjects (48%) in the MNV group and 14 subjects (56%) in the normal controls group endorsed a history of hypertension. In the MNV group, 19 patients were white (83%), 3 were Hispanic (13%) and 1 was Asian (4%). In the normal control group 16 patients were white (70%), 4 were Hispanic (17%) and 3 were Asian (13%).

Mean VA measured 0.28 ± 0.29 logMAR (range, 20/30–20/500 logMAR) and 0.07 ± 0.10 logMAR (range, 20/20–20/30 logMAR) in the treatment-naïve MNV and normal control groups, respectively ($P = 0.0007$). The mean scan quality index was 7.4 and 7.48 in the treatment-naïve MNV and normal control groups, respectively ($P = 0.67$). Most MNV lesions were subfoveal (22 cases [96%]) and smaller than 1 disc diameter. In the treatment-naïve MNV group, the MNV lesion exhibited an average mean area of 0.27 ± 0.25 mm^2 and the associated perilesional DH measured 2.02 ± 1.84 mm^2. The two-way mixed effects intraclass correlation coefficient was 0.95 (95% CI, 0.943–0.958) for the MNV area measurements and 0.94 (95% CI, 0.937–0.957) for the DH area measurements.

Using the Phansalkar local thresholding method, in ring 1, the average CC FD% measured 54.93 ± 5.70 in the MNV group and 42.07 ± 4.60 in the normal control group ($P < 0.0005$). In ring 2, average CC FD% measured 50.18 ± 5.70 in the MNV group and 40.49 ± 4.96 in the normal control group ($P < 0.0005$). The mean CC FD% was significantly greater ($P < 0.0005$) in ring 1 compared with ring 2 in both groups. Moreover, the mean difference in CC FD% between the two rings ring 1 and ring 2 was statistically significantly greater in the AMD eyes compared with the controls: 4.75 ± 4.58 and 1.34 ± 1.19. respectively ($P < 0.001$). (Table 1 and Fig. 5)

Using the standard deviation global thresholding method in ring 1, the average CC FD% measured 38.71 ± 5.70 in the MNV group and 29.81 ± 5.50 in the normal control group ($P < 0.0005$). In ring 2, the average CC FD% measured 35.25 ± 5.50 in the MNV group and 27.31 ± 5.70 in the normal control group ($P < 0.0005$). The mean CC FD% was significantly greater ($P < 0.0005$) in ring 1 compared with ring 2 in both groups. Moreover, the mean difference in CC FD% between the two rings ring 1 and ring 2 was statistically significantly greater in the AMD eyes compared with the controls: 3.45 ± 2.10 and 1.99 ± 1.83 respectively ($P < 0.04$).

In addition, the average CC FD% measured within the peripheral four 1-mm^2 squares using the Phansalkar method was 41.02 ± 3.1 0in MNV eyes and 39.81 ± 3.20 in normal eyes ($P = 0.1$). In the MNV group, the peripheral FD CC % was compared with the CC FD% measured in both ring 1 and ring 2 and the average CC FD% was statistically significantly greater in both rings around the MNV versus the peripheral region ($P < 0.05$)

The exudative and nonexudative subgroups of MNV were also independently compared using both the Phansalkar local thresholding method and the standard deviation global thresholding method. In total, 16 of the 23 eyes (70%, 13 males, 3 females) displayed exudative MNV, whereas 7 of the 23 eyes (30%; 6 males, 1 females) displayed nonexudative MNV. The mean age was 78.93 ± 7.60 years and 86.71 ± 7.60 years in the exudative and nonexudative cohorts, respectively ($P = 0.30$). Mean Snellen VA measured 0.21 ± 0.10 logMAR (range, 20/30–20/500 logMAR) and 0.31 ± 0.30 logMAR (range 20/30–20/50 logMAR) in the exudative and nonexudative cohorts, respectively ($P = 0.20$). The mean scan quality index was 7.35 and 7.50 in the exudative and nonexudative groups, respectively ($P = 0.61$). The mean MNV and perilesional DH area measured 0.26 ± 0.20 mm^2 and 2.32 ± 2.1 mm^2, respectively, in the exudative group, and 0.36 ± 0.30 mm^2 and 1.24 ± 0.80 mm^2, respectively, in the nonexudative cohort. These mean area measurements for MNV and DH were not significantly different when the two groups were compared with *P* values of 0.1 and 0.2, respectively. Demographic data describing the exudative and nonexudative MNV patients are summarized in Table 2.

Using the Phansalkar local thresholding method, in the exudative group, the mean CC FD% was 55.90 ± 5.60 and 50.79 ± 5.65 in ring 1 and ring 2, respectively ($P < 0.001$), whereas the nonexudative cohort exhibited mean CC FD% of 53.01 ± 5.70 and 48.95 ± 6.20 in ring 1 and ring 2, respectively ($P < 0.005$). Although the CC FD percentage was consistently higher (in both rings) in the exudative versus the nonexudative MNV group, these differences were not statistically significant (ring 1 comparison, $P = 0.14$; ring 2 comparison, $P = 0.25$). The mean difference of CC FD%

Investigative Ophthalmology & Visual Science

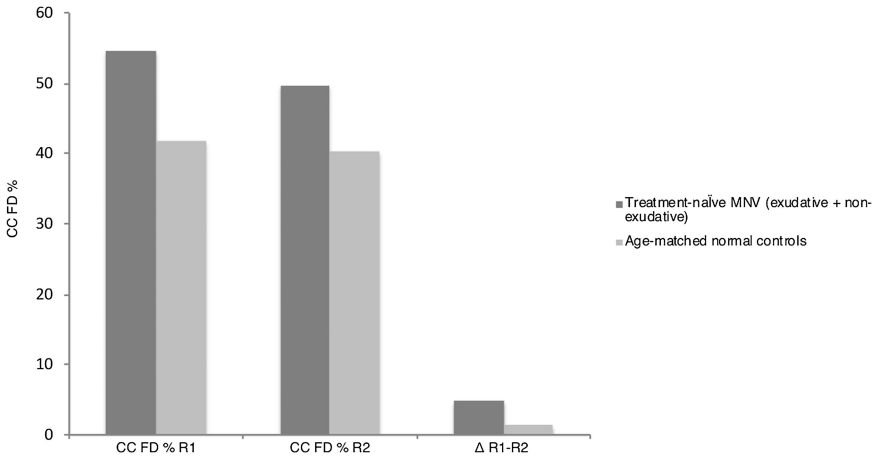

Figure 5. Twenty-three eyes with treatment-naïve MNV were enrolled and age matched with normal controls. Results shown represent the Phansalkar local thresholding method analysis. As illustrated in the graph, the percentage (%) of CC FD is statistically significantly greater in treatment-naïve MNV eyes compared with age-matched normal controls in both ring 1 and ring 2 ($P < 0.0005$). Also, the mean difference of CC FD% between the two rings is statistically significantly greater in the MNV eyes compared with the controls: 4.75 ± 4.58 and 1.34 ± 1.19, respectively ($P < 0.001$).

Table 2. Demographics, VA and MNV Quantitative Data in Exudative versus Nonexudative MNV Cohorts

	Exudative MNV	Nonexudative MNV	*P* Value (*t*-test)
Cases (n)	16	7	–
Age (years ± standard deviation)	78.93 ± 7.60	86.71 ± 7.60	0.30
Sex (M:F)	13:3	6:1	–
VA (LogMAR ± standard deviation; range)	0.21 ± 0.10; 20/30–20/500	0.31 ± 0.30; 20/30–20/50	0.20
Mean MNV (mm^2)	0.26 ± 0.20	0.36 ± 0.30	0.10
Mean dark perilesional halo (mm^2)	2.32 ± 2.10	1.24 ± 0.80	0.20

between the ring 1 and ring 2 did not show any statistical significance in the exudative compared with the nonexudative cohort: 5.11 ± 5.19 and 4.06 ± 2.82, respectively ($P = 0.31$) (Table 3 and Fig. 6).

Using the standard deviation global thresholding method, in the exudative group, the mean CC FD% was 39.69 ± 5.10 and 36.12 ± 4.70 in ring 1 and ring 2, respectively ($P < 0.0005$), whereas the nonexudative cohort exhibited mean CC FD% of 36.7 ± 6.70 and 33.50 ± 6.90 in ring 1 and ring 2, respectively ($P < 0.01$). Although the CC FD percentage was again consistently higher (in both rings) in the exudative versus the nonexudative MNV group, these differences were not statistically significant (ring 1 comparison, $P = 0.16$; ring 2 comparison, $P = 0.19$). The mean difference of CC FD% between the ring 1 and ring 2 did not show any statistically significant difference in the exudative compared with the nonexudative cohort (3.57 and 3.20, respectively; $P = 0.45$).

Eyes from each cohort—exudative and nonexudative—were independently compared with the normal age-matched cohort using the Phansalkar local thresholding method (Fig. 7). For both cohorts, a statistically significant difference in the percentage of CC FD was noted in both ring 1 and ring 2 ($P < 0.05$). We also measured a statistically significant mean difference of the FD CC% between ring 1 and ring 2 in both cohorts.

The intergrader intraclass correlation coefficient for the measurement of MNV and DH areas were 0.91 (95% CI, 0.85–0.93) and 0.87 (95% CI, 0.83–0.93), respectively. The intergrader intraclass correlation coefficient agreement for single measures regarding the quantification of CC FD% in all cohorts using the Phansalkar method in 6 × 6 mm OCTA en face images, was 0.92 (95% CI, 0.89–0.96).

Discussion

In this study, the severity of CC impairment was quantified immediately outside the DH surrounding treatment naive MNV in 23 eyes with AMD versus age-matched controls. The difference in CC FD% was significantly greater in eyes with MNV compared with their age-matched controls in both rings (ring 1 and ring 2) surrounding the DH ($P < 0.05$) using both the Phansalkar and standard deviation global threshold binarization methods. The confounder of regional variation in the CC FD% was accounted for by matching each treatment-naïve MNV eye, one to one, with a normal control from which the same location and area of CC was extracted and analyzed. Further, this study found a significantly greater percentage of CC FD within the 500-µm ring (ring 1) immediately adjacent to the DH compared with ring 2, located 1000 µm from the border of the DH in both groups, but especially in the MNV cohort. A secondary analysis comparing CC FD% in exudative with nonexudative MNV noted an increased FD area in both rings in the exudative MNV group, but this difference was not statistically significant. Each of these results were true for both the Phansalkar and standard deviation global threshold binarization methods.

Investigative Ophthalmology & Visual Science

Table 3. OCT Angiography FD Data for the Exudative MNV versus Nonexudative MNV Cohorts

	CC FD% R1	CC FD% R2	Δ (R1 – R2)	*P* Value
Exudative MNV	55.90 ± 5.60*	50.79 ± 5.65*	5.11 ± 5.19	0.001*
Nonexudative MNV	53.01 ± 5.70†	48.95 ± 6.20†	4.06 ± 2.82	0.005†
P value	0.14	0.25	0.31	–

In the exudative cohort, the mean FD% was 55.90 ± 5.60 and 50.57 ± 5.65, in ring 1 and ring 2, respectively ($P < 0.001$). In the nonexudative cohort, mean FD% was 53.01 ± 5.70 and 48.95 ± 6.20, in ring 1 and ring 2, respectively ($P < 0.005$). Although the CC FD percentage was greater in both rings in the exudative versus the nonexudative groups, this difference was not quite statistically significant. R1 = ring 1; R2 = ring 2.

* Indicates a significant difference between CC FD% R1 and R2 among exudative MNV patients with a p-value of 0.001.

† Indicates a significant difference between CC FD% R1 and R2 among nonexudative MNV patients with a p-value of 0.005.

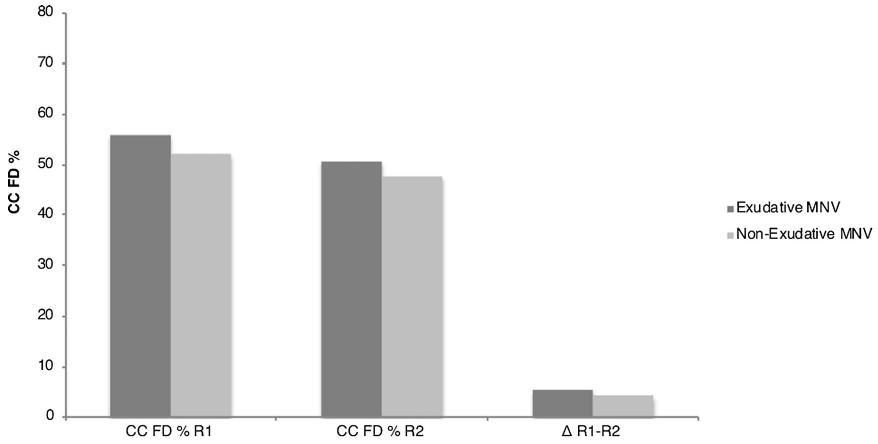

Figure 6. A subanalysis was carried out to compare exudative MNV eyes versus nonexudative MNV eyes. Results shown represent the Phansalkar local thresholding method analysis. The percentage (%) of CC FD is higher in the exudative group for both ring 1 [R1] and ring 2 [R2], but the difference was not statistically significant (ring 1, $P = 0.14$; ring 2, $P = 0.25$). Also, the mean difference of CC FD% between the two rings—ring 1 and ring 2—is not statistically significantly different in the exudative cohort compared with the nonexudative cohort: 5.11 ± 5.19 and 4.06 ± 2.82, respectively ($P = 0.31$).

The present study provides quantitative OCTA evidence that in treatment naïve neovascularization secondary to AMD, the CC is impaired outside of the perilesional halo, indicating that this pathoanatomy may play a role in disease progression. The distribution of CC FD in the area surrounding the DH varies with distance from the margin of the DH, implying that the environment surrounding MNV, especially in the ring immediately surrounding the DH, may be relevant to disease progression.

The importance of CC disease driving MNV is rooted in histopathologic research. In 2009, McLeod et al.[34] described the relationship between the RPE and CC using post mortem eyes of three patients with MNV and illustrated a 50% impairment in the CC immediately surrounding the MNV despite a structurally intact overlying RPE. Biesemeier et al.[35] performed a combined light and electron microscopy study of post mortem specimens from AMD donors and normal controls and showed that CC loss occurs during normal aging and precedes the degeneration of the RPE in eyes with AMD, further indicating that AMD may be a vascular disease.

Recent advances in OCTA and image analysis techniques[36] have demonstrated that CC impairment is greatest in the region surrounding MNV, but these studies were small and descriptive.[1,19,33,37] Recent work by Treister et al.[16] best parallels the current analysis described in this article. The Treister study included FD% in the DH itself (defined as a 200 µm ring around the MNV)[16] and noted a greater CC FD% in the halo, as would be expected. This study was, however, limited by various factors, including the use of 3 × 3 mm scans that were too small to fully encapsulate the MNV in several cases and the inclusion of a heterogeneous group of both treated and treatment-naïve MNV, and the failure to use an image compensation strategy to neutralize shadowing artifacts that can alter the FD analysis. Further, Treister et al. used a 20-µm CC slab to study the CC, which may be inaccurate as the CC is anatomically noted to be 10 µm thick, and analyzed nonexudative lesions in fellow eyes of the same patient, which may introduce bias. Finally, Treister et al. measured the CC FD in a fixed 200-µm area surrounding MNV, which may either over- or underestimate the area of the DH. It is unclear if the DH represents a vascular steal phenomenon of diverted flow through the neovascular lesion or true CC ischemia.[17,38–40] Therefore, our study analyzed the CC directly outside of the DH, excluding the halo itself. Further, in our study 6 × 6 mm scans were used, only treatment-naïve MNV was included, image compensation and superficial vessel masking were utilized, a 10-µm CC slab was studied, no fellow eyes were considered, and two threshold binarization methods were employed.

An analysis of CC health may prove insightful in determining the activity of MNV. With the advent of OCTA,[41] it is not uncommon to encounter nonexudative or quiescent MNV, which does not require anti-VEGF injection. Quiescent MNV typically progresses in area over 12 months. Although

Investigative Ophthalmology & Visual Science

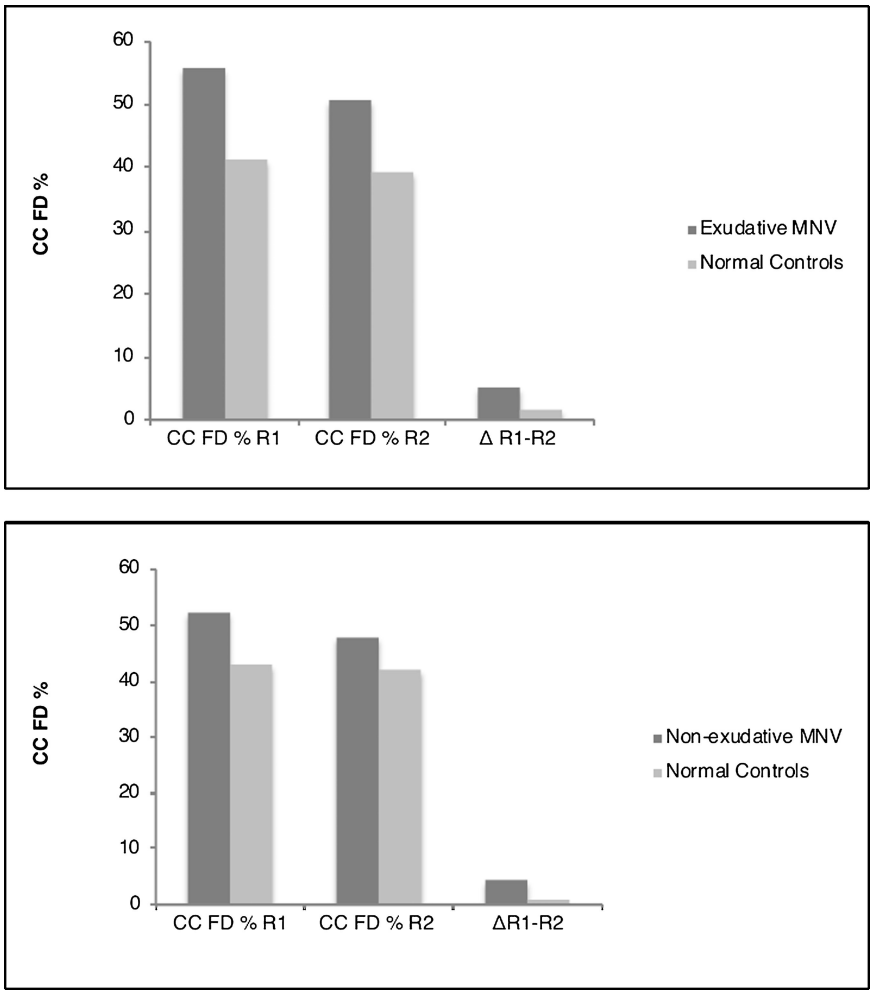

Figure 7. Eyes from the exudative and nonexudative cohorts were compared with their respective age-matched normal controls. Both cohorts display a statistically significant higher percentage of CC FD compared with normal controls. A similar trend is illustrated when quantifying the mean difference between ring 1 [R1] and ring 2 [R2] in both cohorts.

vessel density may remain unchanged, signs of exudation develop in between 6.6% and 26.0% of cases.[42,43] Nonexudative MNV is characterized by a main vessel trunk with intralesional rarefaction of capillaries and less small vessel branching.[44,45] The identification of biomarkers of activity may prove important in predicting which cases of nonexudative MNV will progress to exudation and require anti-VEGF therapy. Exudative MNV may progress and grow at a more rapid rate than nonexudative MNV.[46] Also, the perilesional DH may be identified more commonly in eyes with exudative MNV,[18,45] because active neovascularization may steal adjacent blood flow from surrounding capillaries. In the present study, eyes with exudative MNV showed a larger mean DH area and greater surrounding CC FD than eyes with nonexudative MNV, although these results were not statistically significant. As such, it is possible that the CC may be more compromised in eyes with exudative MNV immediately surrounding the perilesional DH; however, larger prospective studies are necessary to confirm CC viability as a biomarker of MNV activity.

The nature of current OCTA analysis poses some inherent limitations to the current study. A universally accepted and validated approach to quantifying the CC does not yet exist. However, this study applied signal compensation, precise and consistent slab selection, manual and automatic segmentation error correction, and the use of validated local thresholding strategies for FD quantification to maximize reliability. Further, two independent thresholding strategies were applied and consistently validated the outcomes of this investigation.[47,48] High-quality images were not consistently available for each eye, although averaging may improve the quality of the image before quantification of the CC to improve the reliability of FD analysis.[34] Beyond inherent OCTA limitations, the retrospective study design did not allow for a consistent imaging protocol or sequential follow-up. Larger prospective cohorts with longitudinal data will be critical to assess the causative role of these FD in the pathophysiology of neovascular AMD.

In summary, MNV showed a higher percentage of CC FD in the area immediately surrounding the DH versus age-matched normal controls. Moreover, the FD area was consistently greater in the ring closer to the MNV in both AMD and normal eyes. Further, eyes with exudative neovascularization consistently displayed greater CC FD in both rings surrounding the neovascular lesion versus eyes with nonexudative MNV, although this difference was not statistically significant. These findings further support the hypothesis that CC damage may play a primary role in the development

and progression of neovascularization although this awaits further validation with a larger prospective analysis.

Acknowledgments

Supported by Research to Prevent Blindness Inc (DS), New York, New York, and the Macula Foundation Inc (DS, KBF), New York, New York.

Disclosure: **J.M. Scharf,** None; **G. Corradetti,** None; **A.R. Alagorie,** None; **C. Grondin,** None; **A. Hilely,** None; **S. Sadda,** Amgen (C), Allergan (C), Genentech-Roche (C), Oxurion (C), Novartis (C), Regeneron (C), Bayer (C), 4DMT (C), Centervue (C, S), Heidelberg (C, F, S), Optos (C, F, S), Carl Zeiss Meditec (F, S), Nidek (S), Topcon (S); **David Sarraf,** Amgen (C, F), Genentech-Roche (C, 400F), Heidelberg (F), Novartis (C, F), Optovue (C, F), Regeneron (F), Bayer (C, F), Topcon (F)

References

1. Moult EM, Alibhai AY, Rebhun C, et al. Spatial distribution of choriocapillaris impairment in eyes with choroidal neovascularization secondary to age-related macular degeneration. *Retina*. 2020;40:428–445, doi:10.1097/IAE.0000000000002556.
2. Forte R, Coscas F, Serra R, Cabral D, Colantuono D, Souied EH. Long-term follow-up of quiescent choroidal neovascularisation associated with age-related macular degeneration or pachychoroid disease. *Br J Ophthalmol*. 2020;104:1057–1063, doi:10.1136/bjophthalmol-2019-315189.
3. Hayashi K, de Laey JJ. Indocyanine Green Angiography of Choroidal Neovascular Membranes. *Ophthalmologica*. 1985;190:30–39, doi:10.1159/000309489.
4. Bhutto I, Lutty G. Understanding age-related macular degeneration (AMD): relationships between the photoreceptor/retinal pigment epithelium/Bruch's membrane/choriocapillaris complex. *Mol Aspects Med*. 2012;33:295–317, doi:10.1016/j.mam.2012.04.005.
5. Nassisi M, Shi Y, Fan W, et al. Choriocapillaris impairment around the atrophic lesions in patients with geographic atrophy: a swept-source optical coherence tomography angiography study. *Br J Ophthalmol*. 2019;103:911–917, doi:10.1136/bjophthalmol-2018-312643.
6. Moult EM, Waheed NK, Novais EA, et al. Swept-source optical coherence tomography angiography reveals choriocapillaris alterations in eyes with nascent geographic atrophy and drusen-associated geographic atrophy. *Retina*. 2016;36(Suppl. 1):S2–S11, doi:10.1097/IAE.0000000000001287.
7. Alagorie AR, Verma A, Nassisi M, Sadda SR. Quantitative assessment of choriocapillaris flow deficits in eyes with advanced age-related macular degeneration versus healthy eyes. *Am J Ophthalmol*. 2019;205:132–139, doi:10.1016/j.ajo.2019.04.037.
8. Moreira-Neto CA, Moult EM, Fujimoto JG, Waheed NK, Ferrara D. Choriocapillaris loss in advanced age-related macular degeneration. *J Ophthalmol*. 2018;2018:1–6, doi:10.1155/2018/8125267.
9. Green WR, Key SN. Senile macular degeneration: a histopathologic study. *Trans Am Ophthalmol Soc*. 1977;75:180–254.
10. Sarks SH. New vessel formation beneath the retinal pigment epithelium in senile eyes. *Br J Ophthalmol*. 1973;57:951–965, doi:10.1136/bjo.57.12.951.
11. Wong T, Chakravarthy U, Klein R, et al. The natural history and prognosis of neovascular age-related macular degeneration. A systematic review of the literature and meta-analysis. *Ophthalmology*. 2008;115:116–126, doi:10.1016/j.ophtha.2007.03.008.
12. Querques G, Srour M, Massamba N, et al. Functional characterization and multimodal imaging of treatment-naive "quiescent" choroidal neovascularization. *Invest Ophthalmol Vis Sci*. 2013;54:6886–6892, doi:10.1167/iovs.13-11665.
13. Serra R, Coscas F, Boulet JF, et al. Predictive activation biomarkers of treatment-naive asymptomatic choroidal neovascularization in age-related macular degeneration. *Retina*. 2019:40:1224–1233, doi:10.1097/iae.0000000000002604.
14. Spaide RF, Fujimoto JG, Waheed NK, Sadda SR, Staurenghi G. Optical coherence tomography angiography. *Prog Retin Eye Res*. 2018;64:1–55, doi:10.1016/j.preteyeres.2017.11.003.
15. Borrelli E, Sarraf D, Freund KB, Sadda SR. OCT angiography and evaluation of the choroid and choroidal vascular disorders. *Prog Retin Eye Res*. 2018;67:30–55, doi:10.1016/j.preteyeres.2018.07.002.
16. Treister AD, Nesper PL, Fayed AE, Gill MK, Mirza RG, Fawzi AA. Prevalence of subclinical CNV and choriocapillaris nonperfusion in fellow eyes of unilateral exudative AMD on OCT angiography. *Transl Vis Sci Technol*. 2018;7:19, doi:10.1167/tvst.7.5.19.
17. Moult E, Choi W, Waheed NK, et al. Ultrahigh-speed swept-source OCT angiography in exudative AMD. *Ophthalmic Surg Lasers Imaging Retin*. 2014;45:496–505, doi:10.3928/23258160-20141118-03.
18. Coscas GJ, Lupidi M, Coscas F, Cagini C, Souied EH. Optical coherence tomography angiography versus traditional multimodal imaging in assessing the activity of exudative age-related macular degeneration. *Retina*. 2015;35:2219–2228, doi:10.1097/IAE.0000000000000766.
19. Jia Y, Bailey ST, Wilson DJ, et al. Quantitative optical coherence tomography angiography of choroidal neovascularization in age-related macular degeneration. *Ophthalmology*. 2014;121:1435–1444, doi:10.1016/j.ophtha.2014.01.034.
20. Nassisi M, Baghdasaryan E, Tepelus T, Asanad S, Borrelli E, Sadda SR. Topographic distribution of choriocapillaris flow deficits in healthy eyes. Vavvas DG, ed. *PLoS One*. 2018;13:e0207638, doi:10.1371/journal.pone.0207638.
21. Zheng F, Zhang Q, Shi Y, et al. Age-dependent changes in the macular choriocapillaris of normal eyes imaged with swept-source optical coherence tomography angiography. *Am J Ophthalmol*. 2019;200:110–122, doi:10.1016/J.AJO.2018.12.025.
22. Kraus MF, Liu JJ, Schottenhamml J, et al. Quantitative 3D-OCT motion correction with tilt and illumination correction, robust similarity measure and regularization. *Biomed Opt Express*. 2014;5:2591–2613, doi:10.1364/BOE.5.002591.
23. Kraus MF, Potsaid B, Mayer MA, et al. Motion correction in optical coherence tomography volumes on a per A-scan basis using orthogonal scan patterns. *Biomed Opt Express*. 2012;3:1182–1199, doi:10.1364/BOE.3.001182.
24. Garrity ST, Iafe NA, Phasukkijwatana N, Chen X, Sarraf D. Quantitative analysis of three distinct retinal capillary plexuses in healthy eyes using optical coherence tomography angiography. *Invest Ophthalmol Vis Sci*. 2017;58:5548–5555, doi:10.1167/iovs.17-22036.
25. Byon I, Nassisi M, Borrelli E, Sadda SR. Impact of slab selection on quantification of choriocapillaris flow deficits by optical coherence tomography angiography. *Am J Ophthalmol*. 2019;208:397–405, doi:10.1016/j.ajo.2019.08.026.
26. Schneider CA, Rasband WS, Eliceiri KW. NIH Image to ImageJ: 25 years of image analysis. *Nat Methods*. 2012;9:671–675, doi:10.1038/nmeth.2089.
27. Chu Z, Gregori G, Rosenfeld PJ, Wang RK. Quantification of choriocapillaris with optical coherence tomography angiography: a comparison study. *Am J Ophthalmol*. 2019;208:111–123, doi:10.1016/j.ajo.2019.07.003.

28. Zhang Q, Zheng F, Motulsky EH, et al. A novel strategy for quantifying choriocapillaris flow voids using swept-source OCT angiography. *Invest Ophthalmol Vis Sci*. 2018;59:203–211, doi:10.1167/iovs.17-22953.
29. Borrelli E, Shi Y, Uji A, et al. Topographic analysis of the choriocapillaris in intermediate age-related macular degeneration. *Am J Ophthalmol*. 2018;196:34–43, doi:10.1016/j.ajo.2018.08.014.
30. Phansalkar N, More S, Sabale A, Joshi M. Adaptive local thresholding for detection of nuclei in diversity stained cytology images. *2011 International Conference on Communications and Signal Processing, Calicut, 2011*. 2011:218–220, doi:10.1109/ICCSP.2011.5739305.
31. Nassisi M, Tepelus T, Corradetti G, Sadda SR. Relationship between choriocapillaris flow and scotopic microperimetry in early and intermediate age related macular degeneration. *Am J Ophthalmol*. 2020 Apr 28 [Epub ahead of print]. doi:10.1016/j.ajo.2020.04.018.
32. Borrelli E, Uji A, Sarraf D, Sadda SR. Alterations in the choriocapillaris in intermediate age-related macular degeneration. *Investig Ophthalmol Vis Sci*. 2017;58:4792, doi:10.1167/iovs.17-22360.
33. Alagorie AR, Verma A, Nassisi M, Nittala MG, Velaga SS S. Quantitative assessment of choriocapillaris flow voids surrounding choroidal neovascular membranes. *Invest Ophthalmol Vis Sci*. 2019;60:3483.
34. McLeod DS, Grebe R, Bhutto I, Merges C, Baba T, Lutty GA. Relationship between RPE and choriocapillaris in age-related macular degeneration. *Investig Ophthalmol Vis Sci*. 2009;50:4982, doi:10.1167/iovs.09-3639.
35. Biesemeier A, Taubitz T, Julien S, Yoeruek E, Schraermeyer U. Choriocapillaris breakdown precedes retinal degeneration in age-related macular degeneration. *Neurobiol Aging*. 2014;35:2562–2573, doi:10.1016/j.neurobiolaging.2014.05.003.
36. Uji A, Balasubramanian S, Lei J, Baghdasaryan E, Al-Sheikh M, Sadda SR. Impact of multiple en face image averaging on quantitative assessment from optical coherence tomography angiography images. *Ophthalmology*. 2017;124:944–952, doi:10.1016/j.ophtha.2017.02.006.
37. Kashani AH, Chen C-L, Gahm JK, et al. Optical coherence tomography angiography: a comprehensive review of current methods and clinical applications. *Prog Retin Eye Res*. 2017;60:66–100, doi:10.1016/j.preteyeres.2017.07.002.
38. Coscas F, Lupidi M, Boulet JF, et al. Optical coherence tomography angiography in exudative age-related macular degeneration: a predictive model for treatment decisions. *Br J Ophthalmol*. 2019;103:1342–1356, doi:10.1136/bjophthalmol-2018-313065.
39. Forster J, Harriss-Phillips W, Douglass M, Bezak E. A review of the development of tumor vasculature and its effects on the tumor microenvironment. *Hypoxia*. 2017;5:21–32, doi:10.2147/HP.S133231.
40. Rispoli M, Savastano MC, Lumbroso B. Quantitative vascular density changes in choriocapillaris around CNV after anti-VEGF treatment: dark halo. *Ophthalmic Surg Lasers Imaging Retina*. 2018;48:918–924, doi:10.3928/23258160-20181203-02.
41. Carnevali A, Cicinelli MV, Capuano V, et al. Optical coherence tomography angiography: a useful tool for diagnosis of treatment-naïve quiescent choroidal neovascularization. *Am J Ophthalmol*. 2016;169:189–198, doi:10.1016/j.ajo.2016.06.042.
42. Capuano V, Miere A, Querques L, et al. Treatment-naïve quiescent choroidal neovascularization in geographic atrophy secondary to nonexudative age-related macular degeneration. *Am J Ophthalmol*. 2017;182:45–55, doi:10.1016/j.ajo.2017.07.009.
43. Carnevali A, Sacconi R, Querques L, et al. Natural history of treatment-naïve quiescent choroidal neovascularization in age-related macular degeneration using OCT angiography. *Ophthalmol Retin*. 2018;2:922–930, doi:10.1016/j.oret.2018.02.002.
44. Al-Sheikh M, Iafe NA, Phasukkijwatana N, Sadda SR, Sarraf D. Biomarkers of neovascular activity in age-related macular degeneration using optical coherence tomography angiography. *Retina*. 2018;38:220–230, doi:10.1097/IAE.0000000000001628.
45. Wirth MA, Freiberg F, Pfau M, Wons J, Becker MD, Michels S. Optical coherence tomography angiography in age-related macular degeneration: persistence of vascular network in quiescent choroidal neovascularization. *Acta Ophthalmol*. 2017;95:428–430, doi:10.1111/aos.13226.
46. Bailey ST, Thaware O, Wang J, et al. Detection of nonexudative choroidal neovascularization and progression to exudative choroidal neovascularization using OCT angiography. *Ophthalmol Retina*. 2019;3:629–636, doi:10.1016.
47. Mehta N, Liu K, Alibhai AY, et al. Impact of binarization thresholding and brightness/contrast adjustment methodology on optical coherence tomography angiography image quantification. *Am J Ophthalmol*. 2019;205:54–65, doi:10.1016/j.ajo.2019.03.008.
48. Terheyden JH, Wintergerst MW, Falahat P, Berger M, Holz FG, Finger RP. Automated thresholding algorithms outperform manual thresholding in macular optical coherence tomography angiography image analysis. *PLoS One*. 2020;15:e0230260, doi:10.1371.

Investigative Ophthalmology & Visual Science